
Distortion and Residual Stresses during Metal Quenching Process

A.K. Nallathambi¹, Y. Kaymak¹, E. Specht¹, and A. Bertram²

¹Institut für Strömungstechnik und Thermodynamik,
Otto-von-Guericke-Universität Magdeburg

²Institut für Mechanik, Otto-von-Guericke-Universität Magdeburg

Abstract. Quenching is a complex thermo-mechano-metallurgical problem. During the quenching process, transient heat conduction, metallic phase transformations, and plastic behaviour of the metals introduce high residual stresses and distortions. This article presents the mathematical formulation of the physics behind the quenching process, numerical techniques and optimum of cooling strategies for the selected geometries. The Finite Element Method (FEM) is used to solve the coupled partial differential equations in the framework of an isothermal-staggered approach. Coupling effects such as phase transformation enthalpy, transformation-induced plasticity and dissipation are considered. Numerical examples are presented for an L profile made up of 100Cr6 steel.

1 Introduction

Quenching can be defined as *cooling of metals at a rate faster than cooling in still air*. Quenching is physically one of the most complex processes in engineering and very difficult to understand. Quenching used to be called *black hole* of heat treatment processes [1]. Most of the metallic parts have to be quenched after the thermal treatment processes to obtain the required properties such as hardness, micro-structure, etc. Quenching induces high residual stresses due to several mechanisms like phase transformation, thermal shrinkage, and transformation induced plasticity.

The distortion of the L profile can be better understood from Fig. 1, where the distorted shape of the profile is shown at different stages of cooling. Initially due to higher thermal shrinkage at the ends of the legs, the profile bends toward the legs (until 1). However, the ends of the legs soon undergo the phase transition which is also accompanied by a volume increase. Hence, the distortion changes its direction (1-2). As the phase transition penetrates through the legs, the distortion again changes its direction and the profile bends toward the legs one more time (2-3-4). Finally, the phase transition is completed throughout the profile and the distortion gradually decreases as the temperature becomes uniform (4-5). However, a permanent deformation remains due to the mechanical yielding and transformation induced plasticity.

The computer simulation of the quenching process includes three different analyses: (a) Thermal analysis for the computation of cooling curves, (b) Metallurgical analysis for the computation of micro structure composition, and (c) Mechanical analysis for computation of stresses and strains.

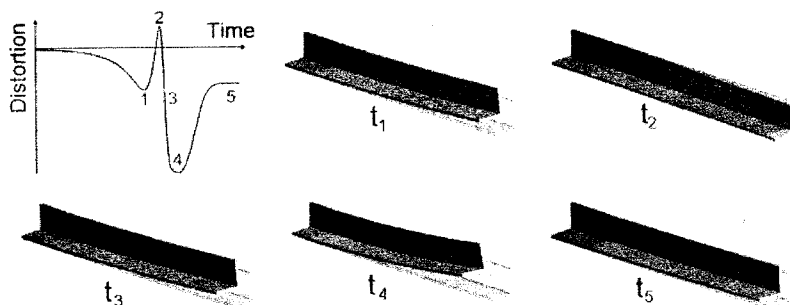


Fig. 1. Distortion of L profile at different stages of quenching

The latent heat released during the phase transformation increases the non-linearity of the problem. The heat flow method [2] is used to model the thermal field, and the FEM is employed for solving the thermal equilibrium equation. In steel like alloys, diffusive and displacive solid-solid phase transformations occur. The diffusive transformation is time-dependent and occurs in the high temperature zone. During the diffusive phase transformation, the parent austenite phase transforms into product phases such as pearlite and bainite. Unlike diffusive, the displacive transformation occurs in the lower temperature zone which is independent of the time. Martensite is the only product of the phase displacive transformation.

The shape change during the quenching process occurs due to the elastic, plastic, thermal phase changes, and transformation induced plastic strains. The complex mechanism behind the residual stress evolution during the quenching process is well explained by Todinov [3]. References [4-8] give more information about the distortion and residual stress calculation during metal quenching. This article is arranged in the following manner: Section 2 presents the mathematical formulation of the three physical fields. The FEM implementation with the isothermal staggered algorithm is described in Section 3. The simulation results are presented with numerical examples in Section 4.

2 Mathematical Formulation

During the quenching process, the temperature, micro-structure, and stresses at every material point change with respect to time. The thermal, metallurgical, and mechanical fields are modelled separately and discussed in this section.

2.1 Thermal Field

Let an open bounded domain $\Omega \subset \mathbb{R}^{n_d}$ ($n_d = 1, 2, 3$) be the configuration of a non-linear thermo-plastic body \mathcal{B} with particles defined by $\bar{X} \in \bar{\Omega}_0$, $\Gamma = \partial\Omega$ its smooth boundary and the time interval of analysis $t \in Y$ ($Y \subset \mathbb{R}^+$). As usual, $\bar{\Omega} = \Omega \cup \Gamma$ and

$\Gamma = \Gamma_\theta \cup \Gamma_q$. The metal quenching problem consists of finding the absolute temperature field $\theta: \tilde{\Omega} \times \Upsilon \rightarrow \mathbb{R}^+$ such that [9]

$$\rho c_p \dot{\theta} = -\nabla \cdot \vec{q} + q_v \quad \text{in } \tilde{\Omega} \times \Upsilon \quad (1)$$

subject to the boundary conditions

$$\theta = \theta_s \quad \text{in } \Gamma_\theta \times \Upsilon \quad (2)$$

$$\vec{q} \cdot \vec{n} = -q_s \quad \text{in } \Gamma_q \times \Upsilon \quad (3)$$

and the initial condition

$$\theta(\vec{X}, t)|_{t=0} = \theta_0(\vec{X}) \quad \text{in } \Omega \quad (4)$$

Eq. (1) represents the energy balance obtained from the first law of thermodynamics. The density ρ and the specific heat capacity c_p , are both functions of the temperature and the phase fraction f_j . The heat generation per unit volume is denoted by q_v , and \vec{q} is the heat flux vector. The internal heat generation accounts for both the phase transformation enthalpies and mechanical energy dissipation

$$q_v = \chi \sigma_y \dot{\varepsilon}^P + \sum_{j=1}^{n_p} L_j \dot{f}_j, \quad (5)$$

where χ is the fraction of mechanical energy converted into thermal energy, σ_y is the yield strength, $\dot{\varepsilon}^P$ is the rate of effective plastic strain, L_j is the latent heat of the individual phase transformation, \dot{f}_j is the phase transition rate and n_p is the number of product phases. In Eq. (0.2), θ_s is the prescribed surface temperature on Γ_θ . On the heat flux boundary Γ_q , q_s is the normal heat flux due to convection-radiation phenomenon. Using the temperature-dependent overall Heat Transfer Coefficient (HTC) α , q_s can be stated according to Newton's law of convection as

$$q_s = -\alpha(\theta)(\theta - \theta_\infty), \quad (6)$$

where θ is the surface temperature, and θ_∞ is the ambient temperature. Fourier's law of heat conduction states that the heat flux vector \vec{q} is proportional to the temperature gradient

$$\vec{q} = -\mathbf{k}(\theta, f_j) \cdot \nabla \theta, \quad (7)$$

where \mathbf{k} is the temperature and phase fraction-dependent second-order thermal conductivity tensor.

2.2 Phase Transformation Field

Phase transformations in solids can be classified as diffusive and displacive transformations. During the transformations in steel, the parent phase austenite may transform into product phases such as pearlite (diffusive) and martensite (displacive).

2.2.1 Diffusive Transformation

The evolution of the diffusive phase transitions is best described by Time-Temperature-Transformation (TTT) diagrams, which are constructed using the isothermal phase change data. The IT (also named TTT) diagrams can be obtained from the Johnson-Mehl-Avrami-Kolmogorov (JMAK) law [10]. In the IT diagram, the double C-curves are plotted for 1% (the transformation start time, t_s) and 99% (the transformation end time, t_e) of the product phase fraction at every temperature θ using the JMAK law. The isothermal formation of the new phase is described by a simple linear iso-kinetic rule [8]

$$\dot{f} = \frac{1}{t_e - t_s}, \quad (8)$$

which states that the rate of phase transformation is constant in the isothermal case. The t_s and t_e can be obtained from the IT diagram. In the non-isothermal case, the cooling curve is considered to be composed of small isothermal steps. The transformation begins at the incubation time t_{inc} , and it ends when the phase fraction reaches unity or the temperature is out of the transformation range. Using Scheil's additivity rule, the incubation time is given as

$$\int_0^{t_{inc}} \frac{1}{t_s(\theta(t))} dt = 1. \quad (9)$$

2.2.2 Displacive Transformation

Shear-dominant, diffusionless, martensitic transformations occur when the temperature of the steel drops rapidly below a critical temperature M_s . Martensite, which is hard and brittle, is a solid solution of carbon in tetragonally, distorted BCC iron. In this work, the displacive transformation is modelled using Koistinen-Marburger's law [8]

$$f_M = f_A \{1 - \exp[k_M(\theta - M_s)]\}, \quad \text{when } \theta < M_s, \quad (10)$$

where f_M and f_A are martensite and austenite phase fractions, M_s is the martensite start temperature and k_M (≈ 0.011) is the stress-dependent transformation constant.

2.3 Displacement Field

A thermo-plastic body \mathcal{B} with interior $\Omega \subset \mathbb{R}^{n_d}$ ($n_d = 1, 2, 3$) and displacement boundary Γ_u , traction boundary Γ_t , $\Gamma = \Gamma_u \cup \Gamma_t$ together as $\tilde{\Omega} = \Omega \cup \Gamma$ and the time interval of analysis $t \in \Upsilon$ ($\Upsilon \subset \mathbb{R}^+$), has to satisfy the equilibrium equation

$$\nabla \cdot \mathbf{T} + \bar{\mathbf{b}} = \bar{\mathbf{0}} \quad \text{in } \tilde{\Omega} \times \Upsilon \quad (11)$$

subject to the boundary conditions

$$\bar{\mathbf{u}} = \bar{\mathbf{u}}_s \quad \text{in } \Gamma_u \times \Upsilon \quad (12)$$

$$\mathbf{T} \cdot \bar{\mathbf{n}} = \bar{\mathbf{t}} \quad \text{in } \Gamma_t \times \Upsilon, \quad (13)$$

where \mathbf{T} is the stress tensor, $\bar{\mathbf{b}}$ is the body force vector, $\bar{\mathbf{u}}_i$ is the prescribed displacement vector, and $\bar{\mathbf{u}}_t$ is the prescribed traction vector with unit outward normal $\bar{\mathbf{n}}$. The total deformation observed in the quenching process is less than 4%. Therefore, using the advantage of small deformation theory, the total strain \mathbf{E} can be additively decomposed into four components as in [6]

$$\mathbf{E} = \frac{1}{2}[\nabla \bar{\mathbf{u}} + (\nabla \bar{\mathbf{u}})^T] = \mathbf{E}^e + \mathbf{E}^p + \mathbf{E}^{tp} + \mathbf{E}^{trip}, \quad (14)$$

where \mathbf{E}^e is the elastic strain tensor, \mathbf{E}^p is the plastic part of strain tensor, \mathbf{E}^{trip} is the Transformation Induced Plastic (TRIP) strain tensor, and \mathbf{E}^{tp} is the volumetric strain tensor due to temperature and phase changes. Once estimating the plastic, the thermal phase change, and the TRIP strain tensors, the elastic strain tensor can be obtained from the total strain tensor, and its methods of estimation are discussed in the subsequent subsections in detail. Using the elastic part of the strain tensor \mathbf{E}^e , the stress tensor \mathbf{T} can be determined from the constitutive law of the material.

2.3.1 Volumetric Thermal Phase Change Strain

During the quenching process, the temperature and phase fractions of the material change drastically. The density of the material undergoing a phase change is a function of the temperature and the phase fractions. For non phase-changing materials like aluminium, copper, nickel, etc, the density depends only on temperature. This nature of varying density produces a reversible strain \mathbf{E}^{tp} . Instead of using the coefficient of thermal expansion, \mathbf{E}^{tp} is expressed in terms of the reference density ρ_R and the current density $\rho(\theta, f_j)$ of the mixture

$$\mathbf{E}^{tp} = \left(\sqrt[3]{\frac{\rho_R}{\rho(\theta, f_j)}} - 1 \right) \mathbf{I}. \quad (15)$$

2.3.2 Transformation Induced Plastic Strain (TRIP)

During the phase change period, austenite may transform into any combination of the following micro-structures: pearlite, bainite and martensite. There is an irreversible strain always associated with the phase change phenomena which is known as TRIP strain, and it is proportional to the stress deviator \mathbf{T}' and the rates of phase transformation \dot{f}_j . Even though the induced stress lies below the yield limit, the TRIP strain occurs in phase changing materials like steel. The TRIP strain rate can be calculated from the macroscopic material behaviour based on the micro-mechanical approach, and it is given as in [8]

$$\dot{\mathbf{E}}^{trip} = -\frac{3}{2} \mathbf{T}' \sum_{j=1}^{n_p} \{ \Lambda_j \ln(f_j) \dot{f}_j \}, \quad (16)$$

where Λ_j is called the Greenwood-Johnson (GJ) coefficient which must be determined experimentally.

2.3.3 Plastic Strain

When the equivalent stress exceeds the yield stress, plastic deformations occur. Using a classical rate-independent, isotropic, thermo-plastic material model with a temperature- and phase fraction-dependent constitutive law, and by systematically employing the yield criterion, loading criterion, flow rule, hardening rule, and consistency condition which are discussed separately in detail, the plastic strain can be estimated. The isotropic constitutive law of the material can be written as in [11]

$$\mathbf{T} = \mathbf{C}^e \cdot \mathbf{E}^e = \kappa \text{tr}(\mathbf{E} - \mathbf{E}^p) \mathbf{I} + 2\mu(\mathbf{E}' - \mathbf{E}'^{trp} - \mathbf{E}^p) \quad (17)$$

where \mathbf{C}^e is the fourth order elasticity tensor, κ is the bulk modulus and μ is the shear modulus, together functions of temperature and phase fractions.

1. **Yield criterion.** The von-Mises yield criterion has the special feature of the smooth surface with convexity which is suitable for pressure-independent ductile materials and given as

$$\phi(\mathbf{T}', \varepsilon^p, T, f_j) = \|\mathbf{T}'\| - \sqrt{\frac{2}{3}} \sigma_y(\varepsilon^p, \theta, f_j), \quad (18)$$

where ε^p is the effective plastic strain which is used as a strain hardening internal variable, and σ_y is the temperature- and phase fractions-dependent yield strength.

2. **Loading criterion.** The loading criterion can be stated as

$$\begin{aligned} \phi = 0 \text{ and } \dot{\phi}|_{\varepsilon^p = \text{const}} &> 0 \text{ loading} \\ \phi = 0 \text{ and } \dot{\phi}|_{\varepsilon^p = \text{const}} &= 0 \text{ neutral loading} \\ \phi = 0 \text{ and } \dot{\phi}|_{\varepsilon^p = \text{const}} &< 0 \text{ unloading} \end{aligned}$$

3. **Flow rule.** An associated flow rule is employed and given as

$$\dot{\mathbf{E}}^p = \dot{\lambda} \frac{\partial \phi}{\partial \mathbf{T}} = \dot{\lambda} \frac{\mathbf{T}'}{\|\mathbf{T}'\|} = \dot{\lambda} \mathbf{n}'_T, \quad (19)$$

where $\dot{\lambda}$ and \mathbf{n}'_T are the plastic multiplier and the flow surface normal or stress deviator direction, respectively.

4. **Hardening rule.** A linear isotropic hardening rule is considered, and the yield strength is stated as in [12]

$$\sigma_y(\varepsilon^p, \theta, f_j) = \sigma_{y_0}(\theta, f_j) + H(\theta, f_j) \varepsilon^p \quad (20)$$

where σ_{y_0} is the yield strength at the virgin state, and H is the plastic modulus. The hardening state variable is integrated from the plastic multiplier

$$\varepsilon^p = \sqrt{\frac{2}{3}} \dot{\lambda} \quad (21)$$

5. **Consistency condition.** In general, the consistency condition $\dot{\phi} = 0$ yields the value of the plastic multiplier $\dot{\lambda}$. The isothermal staggered algorithm [13] suggests that the temperature and phase fractions should be kept constant (i.e., $\dot{\theta} = 0$ and $\dot{f}_j = 0$), so that the plastic multiplier [11] becomes

$$\dot{\lambda} = \frac{2\mu \mathbf{n}'_T \cdot (\dot{\mathbf{E}} - \dot{\mathbf{E}}^{trip})}{2\mu + \frac{2}{3}H} \quad (22)$$

3 Solution Methodology

The non-linear coupled simultaneous equations obtained through FEM are solved using the isothermal staggered algorithm [13]. Thermal, metallurgical and mechanical fields are sequentially solved in every time step in the following way: (a) the thermal field is solved at fixed configuration and phase fractions, (b) the metallurgical field is solved at fixed configuration and constant temperature, (c) the mechanical field is solved at constant temperature and phase fractions. In each time step, first the transient temperature field is solved iteratively, then the phase transitions are computed, and finally the displacement field is computed iteratively. The discrete form of all coupled equations are derived and discussed in detail in the following subsections.

3.1 Thermal Field Formulation

Using FEM, the final matrix form of thermal equilibrium is given as

$$\left\{ \mathbf{K}_i^{\theta t+\Delta t} + \frac{1}{\Delta t} \mathbf{C}_i^{\theta t+\Delta t} \right\} (\Delta \Theta) = \mathbf{F}^{\theta t+\Delta t} - \mathbf{R}_i^{\theta t+\Delta t}, \quad (23)$$

where \mathbf{K}^θ is the global conductance matrix, \mathbf{C}^θ is the global capacitance matrix, \mathbf{F}^θ is the global thermal force vector, and \mathbf{R}^θ is the global residual thermal force vector. The elemental form of these matrices and vectors are given as in [14]

$$\begin{aligned} \mathbf{K}_{e_i}^{\theta t+\Delta t} &= \iint_{\Omega} [\mathbf{H}^T k_i^{t+\Delta t} \mathbf{H}] d\Omega + \int_{\Gamma_q} [\mathbf{N}^S \alpha_i^{t+\Delta t} (\mathbf{N}^S)^T] d\Gamma_q \\ \mathbf{C}_{e_i}^{\theta t+\Delta t} &= \iint_{\Omega} [\mathbf{N} \rho_i^{t+\Delta t} c_{pi}^{t+\Delta t} \mathbf{N}^T] d\Omega \\ \mathbf{F}_{e_i}^{\theta t+\Delta t} &= \iint_{\Omega} [\mathbf{N} q_{vi}^{t+\Delta t}] d\Omega + \int_{\Gamma_q} [\mathbf{N} \alpha_i^{t+\Delta t} \theta_\infty] d\Gamma_q \\ \mathbf{R}_{e_i}^{\theta t+\Delta t} &= \left\{ \iint_{\Omega} [\mathbf{H}^T k_i^{t+\Delta t} \mathbf{H}] d\Omega \right\} \Theta_{e_i}^{t+\Delta t} + \mathbf{C}_{e_i}^{\theta t+\Delta t} \left(\frac{\Theta_{e_i}^{t+\Delta t} - \Theta_{e_i}^t}{\Delta t} \right) \end{aligned} \quad (24)$$

where \mathbf{N} is the element shape function and \mathbf{H} is the element temperature-gradient interpolation operator.

3.2 Phase Field Formulation

At the end of thermal field computation, the current temperature $\Theta^{t+\Delta t}$ and the current temperature increment $\Delta\Theta = \Theta^{t+\Delta t} - \Theta^t$ are known at every integration point of the elements. The displacive and diffusive phase transitions are computed using these temperature details. Martensitic evolution can be directly determined from the Eq. (0.10). Pearlite is considered as the only product of diffusive transformation which is a reasonable simplification. Scheil's sum increment ΔS at the current time step can be computed using the IT diagram information [8]

$$\Delta S = \frac{\Delta t}{t_s^{t+0.5\Delta t}} \quad (25)$$

The current Scheil's sum can be updated to $S^{t+\Delta t} = S^t + \Delta S$. The general phase fraction evolved during the current time step can be given as

$$\Delta f = \frac{\zeta \Delta t}{t_e^{t+0.5\Delta t} - t_s^{t+0.5\Delta t}} \quad (26)$$

The following three possibilities arise in this calculation:

1. If $S^{t+\Delta t} < 1$, then $\Delta f = 0$.
2. If $S^{t+\Delta t} < 1$ and $S^{t+\Delta t} > 1$, the incubation time is reached during the current time step, and only a fraction ζ of Δt contributes to phase transition and $\zeta \approx \frac{S^{t+\Delta t} - 1}{\Delta S}$.
3. If $S^{t+\Delta t} > 1$ and also $S^t > 1$, the phase transition already started and $\zeta = 1$, since the full time step contributes to phase transition.

3.3 Displacement Field Formulation

The final global form of mechanical equilibrium equation becomes

$$\mathbf{K}^{ut+\Delta t} \Delta \hat{\mathbf{U}} = \mathbf{F}^{ut+\Delta t} - \mathbf{R}^{ut+\Delta t}, \quad (27)$$

where \mathbf{K}^u is the global stiffness matrix, \mathbf{F}^u is the global equivalent nodal load vector, \mathbf{R}^u is the internal reaction vector taken from the previous iteration, and $\Delta \hat{\mathbf{U}}$ is the incremental global displacement vector. Elemental forms of matrices and vectors are given as in [14]

$$\begin{aligned} \mathbf{K}_{ei}^{ut+\Delta t} &= \int_{\Omega} [\mathbf{B}^T \mathbf{C}_i^{ept+\Delta t} \mathbf{B}] d\Omega \\ \mathbf{F}_{ei}^{ut+\Delta t} &= \int_{\Gamma_f} [(\mathbf{N}^S)^T \mathbf{t}_e^{t+\Delta t}] d\Gamma_f + \int_{\Omega} [\mathbf{N}^T \mathbf{b}_e^{t+\Delta t}] d\Omega \\ \mathbf{R}_{ei}^{ut+\Delta t} &= \int_{\Omega} [\mathbf{B}^T \mathbf{T}_{ci}^{t+\Delta t}] d\Omega \end{aligned} \quad (28)$$

where \mathbf{t}_e is the boundary element traction vector, \mathbf{b}_e is the element body force vector, \mathbf{B} is the strain-displacement matrix which is unique for the particular structural problem which will be discussed in Section 3.4 \mathbf{C}^{ep} , is the elemental tangent elasto-plastic matrix [11].

3.4 Structural Application

Thermal, metallurgical and mechanical field computations which are discussed in Section 3.1, 3.2 and 3.3 are similar for any kind of a three dimensional metal quenching process except the calculation of strain-displacement matrix \mathbf{B} . The two-dimensional beam problem is considered in this section. Using an iso-parametric element formulation, the global co-ordinates and displacements are given in terms of local co-ordinates (ξ, η) by

$$\begin{aligned} x(\xi, \eta) &= \mathbf{N}^T \mathbf{X}, \quad y(\xi, \eta) = \mathbf{N}^T \mathbf{Y} \\ u(\xi, \eta) &= \mathbf{N}^T \mathbf{U}_e, \quad v(\xi, \eta) = \mathbf{N}^T \mathbf{V}_e \end{aligned} \quad (29)$$

The derivatives of the shape functions with respect to the global x and y co-ordinates are represented by the operator \mathbf{H} of size 2×9 as

$$\mathbf{H} = \begin{bmatrix} \frac{\partial}{\partial x} \\ \frac{\partial}{\partial y} \end{bmatrix} \mathbf{N}^T = \mathbf{J}^{-T} \begin{bmatrix} \frac{\partial}{\partial \xi} \\ \frac{\partial}{\partial \eta} \end{bmatrix} \mathbf{N}^T. \quad (30)$$

The strain-displacement operator \mathbf{B} (subscript 'e' is suppressed) for the plane stress case is the simplest one and it is referred in this text as standard strain-displacement operator with size 3×18 ,

$$\mathbf{B} = \mathbf{B}_{std} = \begin{bmatrix} H_{x1} & 0 & \dots & H_{x9} & 0 \\ 0 & H_{y1} & \dots & 0 & H_{y9} \\ H_{y1} & H_{x1} & \dots & H_{y9} & H_{x9} \end{bmatrix}, \quad (31)$$

where H_x and H_y are the elements of the first and second rows of derivative operator \mathbf{H} . Through the beam cross-sectional element the long profiles can be analyzed by introducing one extra global node with 3 degrees of freedom. The strain-displacement matrix for the beam case [8] has the size 4×21 . There is one additional row and three additional columns. The introduced addition is named as \mathbf{B}_{beam} and

$$\mathbf{B} = \begin{bmatrix} \mathbf{B}_{std} & \mathbf{0} \\ \mathbf{0} & \mathbf{B}_{beam} \end{bmatrix}, \quad \text{where } \mathbf{B}_{beam} = \frac{1}{l} [1 \quad y \quad -x]. \quad (32)$$

The additional operator \mathbf{B}_{beam} is only for computing the strain in the axial direction, which is just related to axial elongation w and bending curvatures c_x and c_y . The standard elasto-plastic stress-strain operator is given as

$$\hat{\mathbf{C}}_{std}^{ep} = 3\kappa \hat{\mathbf{P}}_1 + 2\mu \hat{\mathbf{P}}_2 - \frac{2\mu}{1 + \frac{H}{3\mu}} \hat{\mathbf{n}}_T' - \lambda \frac{4\mu^2}{\|(\mathbf{T}')^{trial}\|} \left(\hat{\mathbf{P}}_2 - \hat{\mathbf{n}}_T' \right), \quad (33)$$

where $\hat{\mathbf{P}}_1$ is the spherical projector, $\hat{\mathbf{P}}_2$ is the deviator projector, and $\hat{\mathbf{n}}_7'$ is the plastic flow direction projector. The projectors are of size 4x4

$$\hat{\mathbf{P}}_1 = \frac{1}{3} \begin{bmatrix} 1 & 1 & 0 & 1 \\ 1 & 1 & 0 & 1 \\ 0 & 0 & 0 & 0 \\ 1 & 1 & 0 & 1 \end{bmatrix}, \quad \hat{\mathbf{P}}_2 = \frac{1}{2} \begin{bmatrix} \frac{4}{3} & \frac{-2}{3} & 0 & \frac{-2}{3} \\ \frac{-2}{3} & \frac{4}{3} & 0 & \frac{-2}{3} \\ 0 & 0 & 1 & 0 \\ \frac{-2}{3} & \frac{-2}{3} & 0 & \frac{4}{3} \end{bmatrix} \quad (34)$$

4 Results and Discussions

An L120x12 profile made up of 100Cr6 steel of unit length is modeled using the beam cross-sectional elements as discussed in the Section 3.4. The temperature-dependent material properties of the individual phases can be found in reference [6]. The distortion of the long profiles is represented by their curvature. The volume averages of the temperature and the effective stresses are considered for the comparison of different cooling strategies.

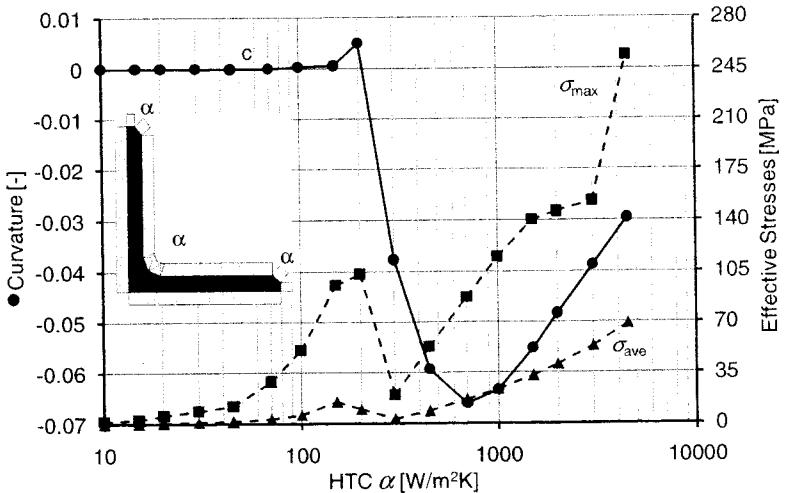


Fig. 2. HTC α vs. Curvature and Effective stresses in equal cooling of L-100Cr6

A series of simulations with equal HTC (α) ranging from 10-4500W/m²K has been performed to find out the critical cooling regions. The computed final distortion, the average and the maximum effective stresses are plotted against α in Fig.2. In the low cooling range $\alpha < 200$ W/m²K no distortion is observed, that it increases in the negative direction, reaches maximum at $\alpha = 700$ W/m²K, and afterward changes its cooling range and they reaches a local maximum where the distortion of the profile is

direction. The internal stresses gradually increase with the increasing α in the low first observed. Next, a local minimum of stress indicates that the different parts of the profile are plastified in the reverse direction which produces the distortion but at the same time relaxes the residual stress state.

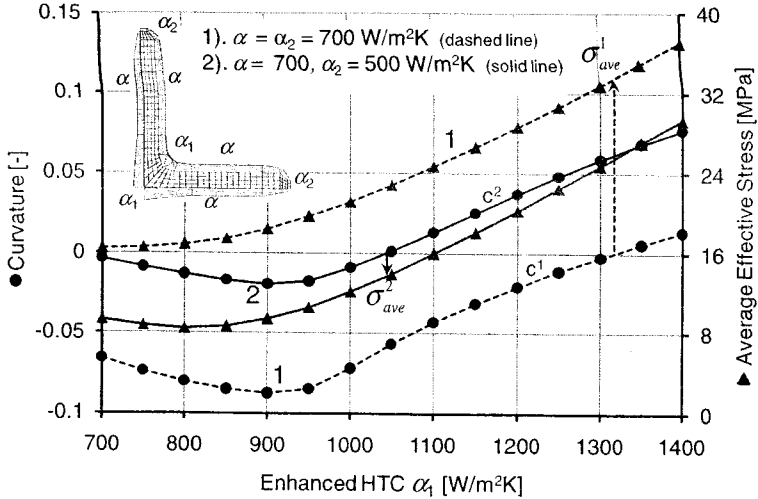
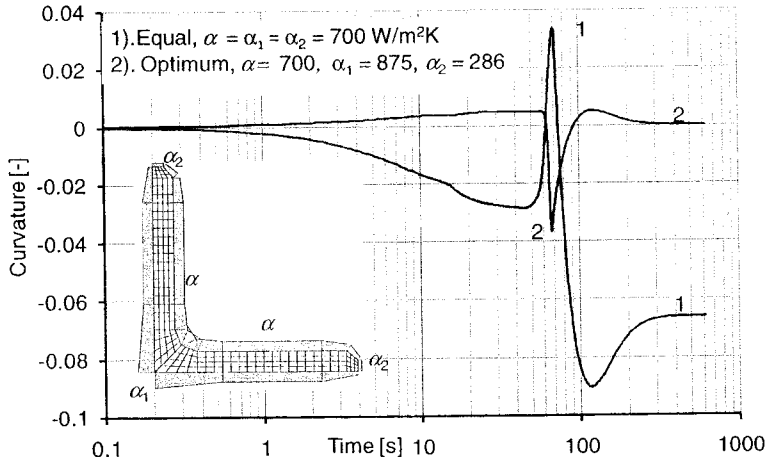


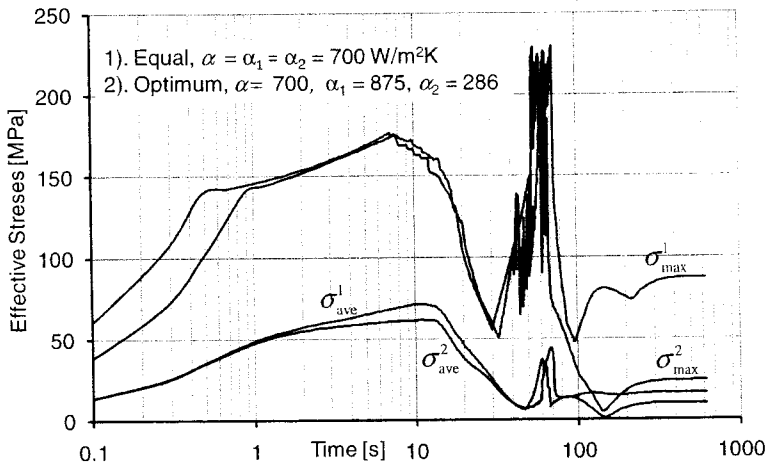
Fig. 3. Curvature and average effective stress as a function of enhanced HTC α_1 (L-100Cr6)

During an equal cooling, the temperature gradient is not uniform due to the mass distribution with respect to the locations of the boundaries. The distortion can be eliminated by increasing the local cooling at mass lumped regions [6]. This fact is verified in this section with the first cooling strategy as shown in Fig. 3. Firstly, increasing the HTC only at the mass lumped region moderately equalizes the temperature distribution. The HTC at the mass lumped region is designated by α . As the HTC α_1 is increased, the distortion gets reduced and totally eliminated at $\alpha_1 = 1315 \text{ W/m}^2\text{K}$. Further increase in the HTC α_1 produces a distortion in the reverse direction. However, this strategy increases the residual stress continuously as shown in Fig. 3. From this simulation result, one can come to the conclusion that increasing the HTC at the mass lumped region can only reduce the distortion but not the residual stresses.

Secondly, reducing the cooling at the edges and enhancing the cooling at the mass lumped region equalizes the temperature distribution inside the material to a greater extent [7]. To implement this, strategy 2 in which $\alpha_2 = 500 \text{ W/m}^2\text{K}$ is maintained at the edges along with uniform cooling $\alpha = 700 \text{ W/m}^2\text{K}$ is introduced. The curvature and the stresses are plotted for various values of enhanced cooling HTC α_1 . The distortion is completely eliminated when α_1 reaches $1040 \text{ W/m}^2\text{K}$. The residual stress at



(a) Curvature evolution



(b) Effective stresses evolution

Fig. 4. Comparisons: equal and optimum cooling strategies - curvature and stresses evolution

zero curvature in strategy 2 is half the value of strategy 1. This fact indicates that with a continent combination of α_1 and α_2 , it is a possible to reduce the residual stresses at a distortion free final state.

For $\alpha = 700\text{W/m}^2\text{K}$, the values of α_1 and α_2 are identified through a standard two parameter optimisation technique. In the case of the optimum cooling strategy, the distortion is much smaller during the cooling and it is finally eliminated as shown in Fig. 4a. The final maximum equivalent stress is reduced approximately from 87.2 to 24MPa. Similarly, the average effective stress is reduced from 16.4 to 10.1MPa as

shown in Fig. 4b. During the phase transformation the maximum equivalent stress fluctuates a lot due to the transformation induced plasticity.

5 Concluding Remarks

The metal quenching process is analysed using a non-linear finite element technique which includes the coupling of the thermal, metallurgical and mechanical fields within the frame of the isothermal staggered approach. The distortion and residual stress evolution are calculated for long **L** profile made of steel. Along with an enhanced cooling at the mass lumped region, a reduced cooling at the edges and corners simultaneously reduces both the distortion and the residual stresses.

References

- [1] Smoljan, B.: Numerical simulation of steel quenching. *J. Mat. Engg. Perf.* 11, 75–79 (2002)
- [2] Lewis, R.W., Ravindran, K.: Finite element simulation of metal casting. *Int. J. Num. Meth. Engg.* 47, 29–59 (2000)
- [3] Todinov, M.T.: Mechanism for formation of the residual stresses from quenching. *Model. Sim. Mat. Sci. Engg.* 6, 273–291 (1998)
- [4] Pietzsch, R., Brzoza, M., Kaymak, Y., Specht, E., Bertram, A.: Minimizing the distortion of steel profiles by controlled cooling. *Steel Res. Int.* 76, 399–407 (2005)
- [5] Brzoza, M., Specht, E., Ohland, J., Belkessam, O., Lübben, T., Fritsching, U.: Minimizing stress and distortion for shafts and discs by controlled quenching in a field of nozzels. *Mat. Sci. Engg. Tech.* 37, 97–102 (2006)
- [6] Pietzsch, R., Brzoza, M., Kaymak, Y., Specht, E., Bertram, A.: Simulation of the distortion of long steel profiles during cooling. *J. App. Mech.* 74, 427–437 (2007)
- [7] Kaymak, Y., Specht, E.: Strategies for controlled quenching to reduce stresses and distortion. *Heat Proces.* 5(3), 1–4 (2007)
- [8] Kaymak, Y.: Modeling of metal quenching process and strategies to minimize distortion and stresses, PhD thesis, Otto-von-Guericke University, Magdeburg, Germany (2007), <http://diglib.uni-magdeburg.de/Dissertationen/2007/yalkaymak.pdf>
- [9] Celentano, D., Orate, E., Oller, S.: A temperature-based formulation for finite element analysis of generalized phase-change problems. *Int. J. Num. Meth. Engg.* 37, 3441–3465 (1994)
- [10] Kang, S.H., Im, Y.T.: Finite element investigation of multi-phase transformation within carburized carbon steel. *J. Mat. Proc. Tech.* 183, 241–248 (2007)
- [11] Simo, J.C., Hughes, T.J.R.: *Computational Inelasticity*. Springer, New York (1997)
- [12] Chen, W.-F.: *Constitutive Equations for Engineering Materials. Plasticity and Modelling*, vol. 2. Elsevier, Netherlands (1994)
- [13] Armero, F., Simo, J.C.: A new unconditionally stable fractional step method for nonlinear coupled thermomechanical problems. *Int. J. Num. Mct. Engg.* 35, 737–766 (1992)
- [14] Bathe, K.J.: *Finite Element Procedures*. Prentice-Hall Inc., New Jersey (1996)

Albrecht Bertram
Jürgen Tomas

Micro-Macro-Interactions

In Structured Media and Particle Systems